Author(s): Välikangas, Juho; Laine, Petteri; Hu, Tao; Tynjälä, Pekka; Selent, Marcin; Molaiyan, Palanivel; Jürgen, Kahr; Lassi, Ulla

Title: Effect of Secondary Heat Treatment after a Washing on the Electrochemical Performance of Co-Free LiNi0.975Al0.025O2 Cathodes for Li-Ion Batteries

Year: 2024

Version: Published version

Please cite the original version:

Välikangas, J., Laine, P., Hu, T., Tynjälä, P., Selent, M., Molaiyan, P., Jürgen, K., & Lassi, U. (2024). Effect of Secondary Heat Treatment after a Washing on the Electrochemical Performance of Co-Free LiNi0.975Al0.025O2 Cathodes for Li-Ion Batteries. Small, 20(4), Article 2305349. https://doi.org/10.1002/smll.202305349

Nanoelectronics and Its New Materials – A NEW ERA OF NANOSCIENCE

Nanoelectronics and Its New Materials –
A NEW ERA OF NANOSCIENCE

ZEISS
Seeing beyond

WILEY
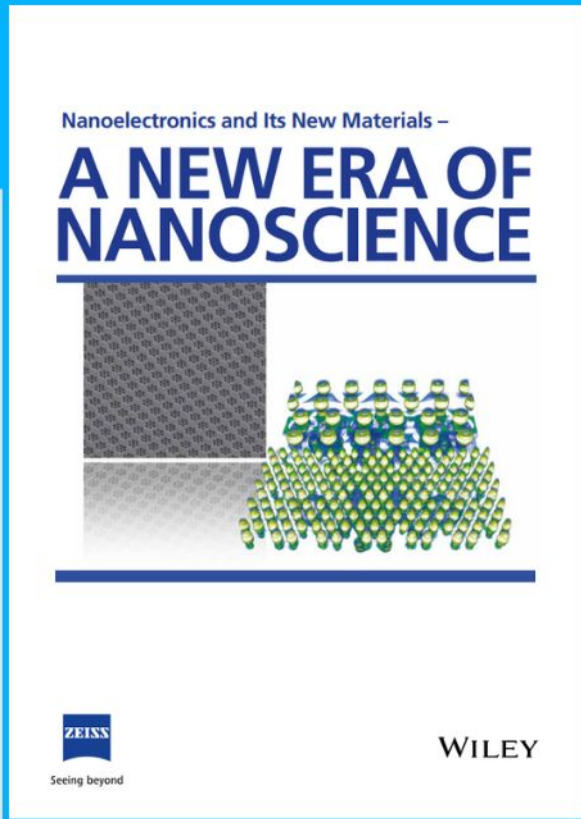
Discover the recent advances in electronics research and fundamental nanoscience.

Nanotechnology has become the driving force behind breakthroughs in engineering, materials science, physics, chemistry, and biological sciences. In this compendium, we delve into a wide range of novel applications that highlight recent advances in electronics research and fundamental nanoscience. From surface analysis and defect detection to tailored optical functionality and transparent nanowire electrodes, this eBook covers key topics that will revolutionize the future of electronics.

To get your hands on this valuable resource and unleash the power of nanotechnology, simply download the eBook now. Stay ahead of the curve and embrace the future of electronics with nanoscience as your guide.

ZEISS

Seeing beyond

WILEY

Effect of Secondary Heat Treatment after a Washing on the Electrochemical Performance of Co-Free LiNi$_{0.975}$Al$_{0.025}$O$_2$ Cathodes for Li-Ion Batteries

Juho Välikangas, *Petteri Laine, Tao Hu, Pekka Tynjälä, Marcin Selent, Palanivel Molaiyan,* *Kahr Jürgen, and Ulla Lassi**

The steadily growing electric vehicle market is a driving force in low-cost, high-energy-density lithium-ion battery development. To meet this demand, LiNi$_{0.975}$Al$_{0.025}$O$_2$ (LNA), a high-energy-density and cobalt-free cathode material, has been developed using a low-cost and efficient co-precipitation and lithiation process. This article explores how further processing (i.e., washing residual lithium from the secondary particle surface and applying a secondary heat treatment at 650 °C) changes the chemical environment of the surface and the electrochemical performance of the LNA cathode material. After washing, a nonconductive nickel oxide (NiO) phase is formed on the surface, decreasing the initial capacity in electrochemical tests, and suppressing high-voltage (H2) to (H3) phase transition results in enhanced cycle properties. Furthermore, the secondary heat treatment re-lithiates surface NiO back to LNAand increases the initial capacity with enhanced cycle properties. Electrochemical tests are performed with the cells without tap charge to suppress the H2 to H3 phase transition. Results reveal that avoiding charging cells at a high voltage for a long time dramatically improves LNA's cycle life. In addition, the gas analysis tests performed during charge and discharge to reveal how the amount of residual lithium compounds on the surface affects gas formation are studied.

1. Introduction

Lithium cobalt oxide (LiCoO$_2$)[1] has long been the most used cathode material in lithium-ion batteries (LIBs). This material is especially popular for portable electronics because of its high energy density. Increased demand for LIBs, especially for use in electric vehicles, has been the driving force in efforts to replace rare and expensive cobalt in cathodes.[2] Cobalt is most replaced with nickel and manganese in LiNi$_{x-y-z}$Co$_y$Mn$_x$O$_2$ (NCM) or with nickel and aluminum in LiNi$_{x-y-z}$Co$_y$Al$_x$O$_2$ (NCA); however, a wide range of metal ratios are produced.[3]

High-nickel cathodes are attractive because the increased amount of nickel in the structure increases the specific capacity of the cathode material.[4,5] However, there are several problems with this ratio, including Li/Ni mixing during synthesis, poor electrochemical cycling stability, and thermal instability.[6–10] During the high-temperature lithiation process, excess lithium is used to suppress Li/Ni mixing and compensate for lithium evaporation during the synthesis. Lithium excess led to high amount of residual lithium compounds, such as lithium carbonate (Li$_2$CO$_3$) and lithium hydroxide (LiOH), on the secondary particle surface.[11] Moreover, the amount of Li$_2$CO$_3$ on the high-nickel cathode surface could increase after synthesis if the surface is exposed to air. Since Ni^{3+} has lower chemical stability than Co^{3+}, the high-nickel cathode surface is more sensitive

J. Välikangas, P. Laine, T. Hu, P. Tynjälä, P. Molaiyan, U. Lassi
Research Unit of Sustainable Chemistry
University of Oulu
P.O. Box 4000, Oulu FI-90014, Finland
E-mail: juho.valikangas@oulu.fi; palanivel.molaiyan@ait.ac.at;
ulla.lassi@oulu.fi

J. Välikangas, P. Laine, P. Tynjälä, U. Lassi
Applied Chemistry
University of Jyvaskyla, Kokkola University Consortium Chydenius
Talonpojankatu 2B, Kokkola FI-67100, Finland
M. Selent
Centre for Material Analysis
University of Oulu
P.O. Box 4000, Oulu FI-90014, Finland
P. Molaiyan, K. Jürgen
AIT Austrian Institute of Technology GmbH
Center for Low-Emission Transport
Battery Technologies
Giefinggasse 2, Vienna 1210, Austria

**ADVANCED
SCIENCE NEWS**

www.advancedsciencenews.com
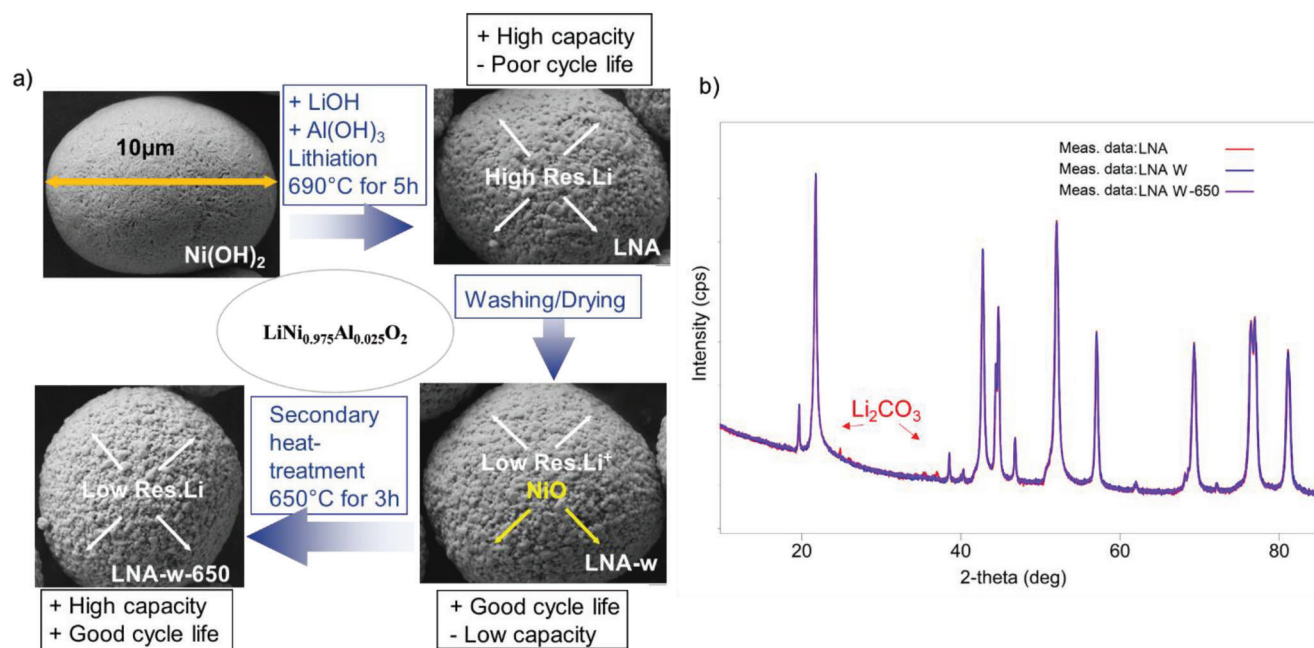
NANO · MICRO

small

www.small-journal.com

Figure 1. a) A schematic of cobalt-free LNA cathode synthesis via Co-precipitation and solid-state method, b) XRD patterns of the pristine (LNA), washed (LNA-w), and secondary heat-treated (LNA-w-650) samples.

to moisture and carbon dioxide. As such, lithium (Li) and oxygen (O_2) from the structure react with carbon dioxide (CO_2), forming thin layers of NiO and Li_2CO_3 on the surface.

The amount of residual lithium compounds on the surface is critical for electrochemical performance. The compounds can react with the electrolytes during the electrochemical reaction and accelerate the formation of hydrofluoric acid (HF), which, in turn, can form insulating layers and decrease electrochemical performance. Furthermore, a high amount of electrolyte decomposing gases can lead to cell swelling, bad electrochemical performance, and cell failure. In addition, moisture-sensitive residual lithium compounds can lead to cathode slurry gelation and difficulties in the electrode fabrication process.[12–18]

In a previous paper, we showed that, compared to pure lithium nickel oxide ($LiNiO_2$), aluminum-modified LNA is an attractive candidate for next-generation cathode material in LIBs because it has a high capacity (215 mAh g^{-1}) at a reasonable voltage range (4.2–2.6 V) and moderate cycling stability after washing process.[19] During the washing, most residual Li_2CO_3 and LiOH compounds that originated from the lithiation process are washed from the surface, and a thin layer of delithiated phase NiO forms on the surface of $LiNiO_2$. The washing process is more challenging for the pure $LiNiO_2$ than those containing cobalt because Ni^{3+} has lower chemical stability than Co^{3+}.[12]

Washing and secondary heat treatment increase the manufacturing costs of the cathode material. However according to Ahmed et al., for NCM cathode material annual costs of purchased capital equipment are 1.4% and utilities (Electricity, Natural gas, and water) are only 1%, however same time raw material costs are 54%. Price of the cobalt is much higher than nickel so it's obvious that minimizing the amount of cobalt even with new process steps is economically beneficial.[20]

In this work, the effects of washing on the chemical structure on the material surface determine how that will affect electrochemical performance and gas formation during the cycling tests. After washing, a secondary heat treatment is performed with the aim to restore the surface structure and the electrochemical performance. Yoon et al. show that H2 to H3 phase transition could be avoided by lowering the charge cutoff voltage.[21] Recently Guo et al. show that electrolytes with low surface reactivity with LNO at a high state of charge can increase the cycle life of LNO/Li cells.[3] Furthermore, our studies show that modifying the charging protocol was identified as an effective way to suppress the H2 to H3 phase transition and dramatically improve capacity retention in full cell tests.

2. Results and Discussion

2.1. Effect of Washing and Secondary Heat Treatment of LNA Cathode Material

2.1.1. Structural and Morphology Investigations of LNA

XRD patterns for LNA cathodes are shown in **Figure 1**b. They indicated that the pristine (LNA), washed (LNA-w), and secondary heat-treated (LNA-w-650) samples had an α-NaFeO$_2$-type structure that was similar to that of the R3m space group (ICDD: 04-023-9746). Small peaks indexed for Li_2CO_3 were detected only for unwashed LNA shown in Figure 1b and Figure S1a (Supporting Information). The lattice parameters and Ni occupations on the Li site obtained from the XRD data are shown in **Table 1** and Table S1 (Supporting Information). The lattice parameters for LNA-w increased slightly; however, these changes might be due to the removal of residual lithium and impurities from the surfaces as a
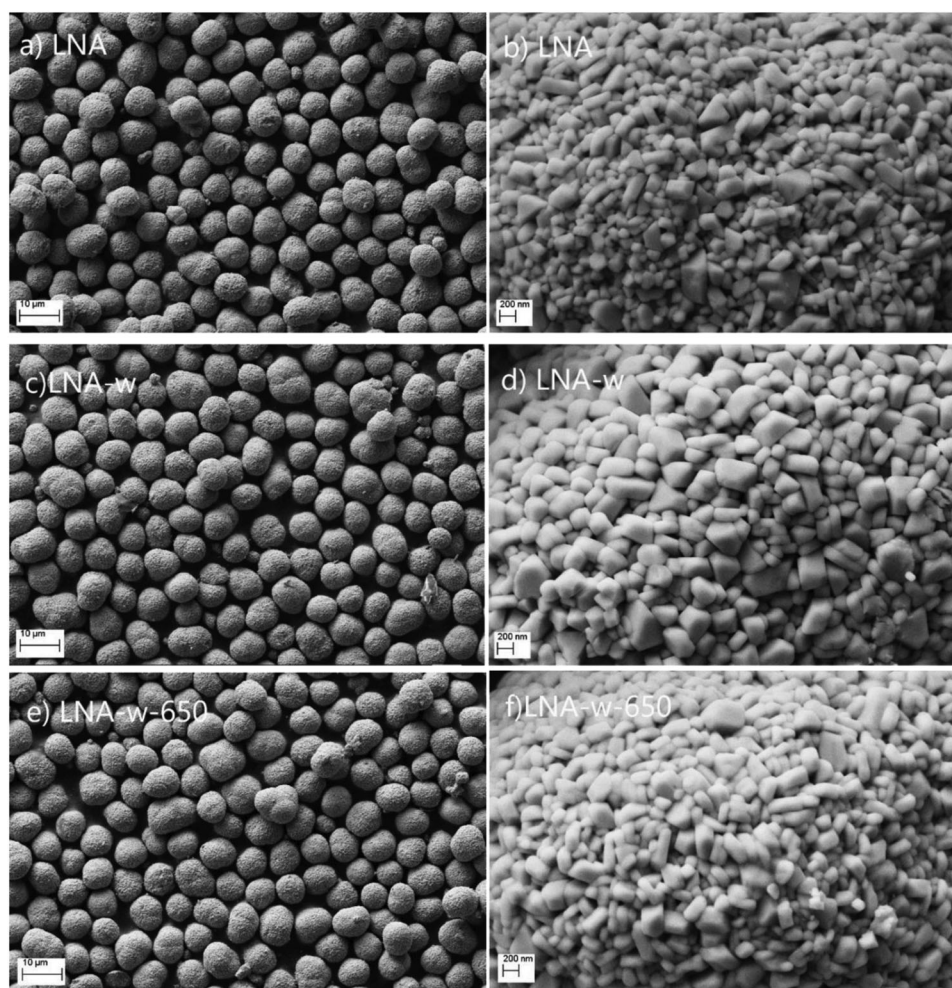
**ADVANCED
SCIENCE NEWS**

www.advancedsciencenews.com

**NANO · MICRO
small**

www.small-journal.com

Figure 2. FESEM images of a,b) pristine LNA, c,d) washed LNA-w, and e,f) wash and heat-treated LNA-w-650. The FESEM morphology at 10 um and 200 nm.

result of washing. In other words, washing may not have changed the unit size of the material. XPS analyses revealed an increased amount of NiO phase on the LNA-w surface, which could have slightly affected the lattice parameters. For LNA-w-650, lattice parameters slightly increase, and the amount of nickel increase in the Li site, indicating that a lower amount of lithium on the second heat-treatment increase the disorder in the layered structure.

Table 1. Cell parameters of the pristine (LNA), washed (LNA-w), and secondary heat-treated (LNA-w-650) samples. The error in lattice parameter 2.87536(2) means ± 0.00002.

Parameters[a]	Unit	LNA	LNA-w	LNA-w-650
c-axis	Å	14.1983(2)	14.2011(2)	14.2059(2)
a-axis	Å	2.87536(2)	2.87552(2)	2.87621(2)
$c/3a$		1.6460	1.6462	1.6464
Crystallite size a	Å	1802.57	1935.15	2201.84
Crystallite size c	Å	2516.04	2681.92	2902.31
Ni on Li site		0.0220	0.0250	0.032

As expected, the crystal size also increased during secondary heat treatment.

As shown in **Figure 2**, all prepared materials had a round-shaped secondary particle morphology that was about 8 µm diameter. Moreover, 50 000 magnifications revealed that the secondary particles consisted of primary particles of about 200 nm. Washing and secondary heat treatment did not affect particle morphology, indicating that impurities and different amounts of residual lithium compounds formed a few nanometer-thin layers on the particle surface that could not be detected in FESEM images. Kim et al. and Zhuang et al. reported similar observations for the residual lithium compounds on the NCA type cathode material.[13,14] As shown in **Table 2**, the ICP-OES results revealed that sulfur, sodium, and other impurities were present on the unwashed material surface and effectively removed by the washing process. Titration analysis (Li wt%) and the Li/Me ratio measured using ICP-OES revealed that washing removed most residual Li_2CO_3 and LiOH compounds from the secondary particle surface. There was a low level of residual lithium compounds in LNA-w. LNA-w-650, which had a secondary heat treatment at 650 °C in an O_2 atmosphere, had a higher concentration

Table 2. Li_2CO_3, LiOH, and Li concentrations on particle surfaces (detected by titration analysis) and Li, Ni, Co, Al, Mn, S, and Na concentrations and the Li/Me ratio (detected by ICP-OES).

Sample	Li_2CO_3 [wt%]	LiOH [wt%]	Li [wt%]	Ni [mol%]	Co [mol%]	Al [mol%]	S [mg g^{-1}]	Na [mg g^{-1}]	Li/Me Ratio
LNA	1.65	0.85	0.56	97.5	0.016	2.5	1.87	0.14	1.073
LNA-w	0.46	0.01	0.09	97.4	0.016	2.6	0.14	0.05	1.020
LNA-w-650	0.44	0.35	0.18	97.4	0.015	2.5	0.14	0.05	1.034

of residual lithium compounds, indicating that heat treatment accelerated the formation of Li_2CO_3 and LiOH on the surface. Xiong et al. obtained similar post-washing results when studying secondary heat-treated $LiNi_{0.8}Co_{0.1}Mn_{0.1}O_2$ (NMC811) cathode material.[22]

Surface compounds and oxidation states were further analyzed using XPS. **Figure 3**a–c shows the O1s spectra analysis of LNA, LNA-w, and LNAw-650. For LNA, the highest peak (531.6 eV) was assigned to CO_3 and OH species, indicating high amounts of residual Li_2CO_3 and LiOH compounds on the surface. A lower peak (529.1 eV) was assigned to lattice oxygen in the metal framework. For LNA-w, the highest peak was assigned to lattice oxygen in the metal framework, indicating that residual LiOH compounds were completely washed away because of their high solubility in water. Most of the Li_2CO_3 compounds, which were less soluble, were also washed away. The surface analysis of LNA-w-650 confirmed the titration results in Table 2; the amount of residual lithium compounds on the surface was higher for LNA-w-650 than for LNA-w. However, this amount was not as high as the amount for LNA.

As shown in Figure 3d–f, the Ni 2p spectra analysis for LNA revealed a low count level due to the high amount of residual lithium compounds on the surface. After washing residual lithium compounds, the Ni 2p spectra analysis showed a higher count level for LNA-w compared to LNA. The Ni $2p_{3/2}$ peak was fitted in Ni^{2+} (854.4 eV), indicating a delithiated phase NiO,[23] and Ni^{3+} (856 eV) from the LNA structure.[12] Unlike LNA, LNA-w's Ni^{2+} peak was higher than its Ni^{3+} peak, indicating that a high amount of delithiated phase NiO formed on the surface with the reaction of H_2O and $LiNiO_2$.[22] However, after secondary heat treatment, the level of Ni^{2+} decreased compared to Ni^{3+}, indicating that NiO was oxidized and re-lithiated with existing Li compounds on the surface to $LiNiO_2$.[12,22]

2.1.2. Electrochemical Performance of LNA

As shown in **Figure 4**a, the electrochemical results from the full cell tests confirmed that an increased amount of NiO phase on the LNA-w surface decreased ionic conductivity and resulted in an initial capacity of 187.6 mAh g^{-1} (compared to 203.1 mAh g^{-1}
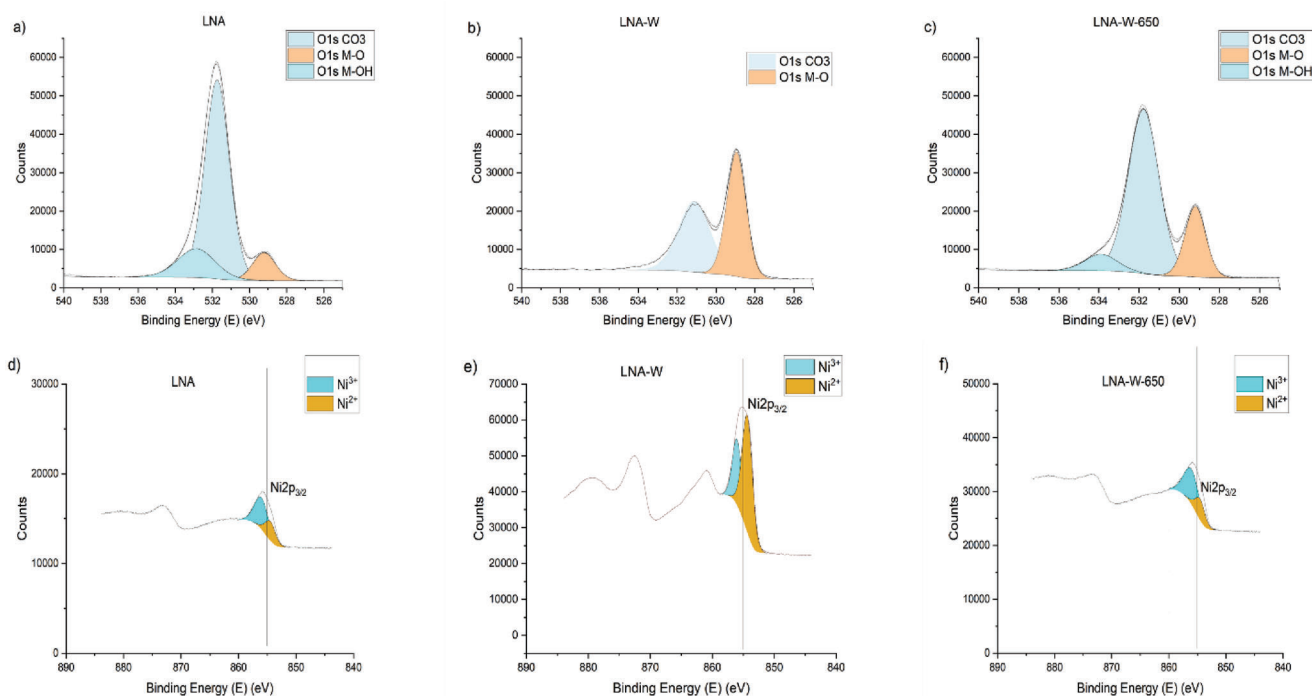

Figure 3. XPS spectra of a–c) O1s and d–f) Ni2p for pristine (LNA), washed (LNA-w), and secondary heat-treated (LNA-w-650) samples.

ADVANCED
SCIENCE NEWS

www.advancedsciencenews.com
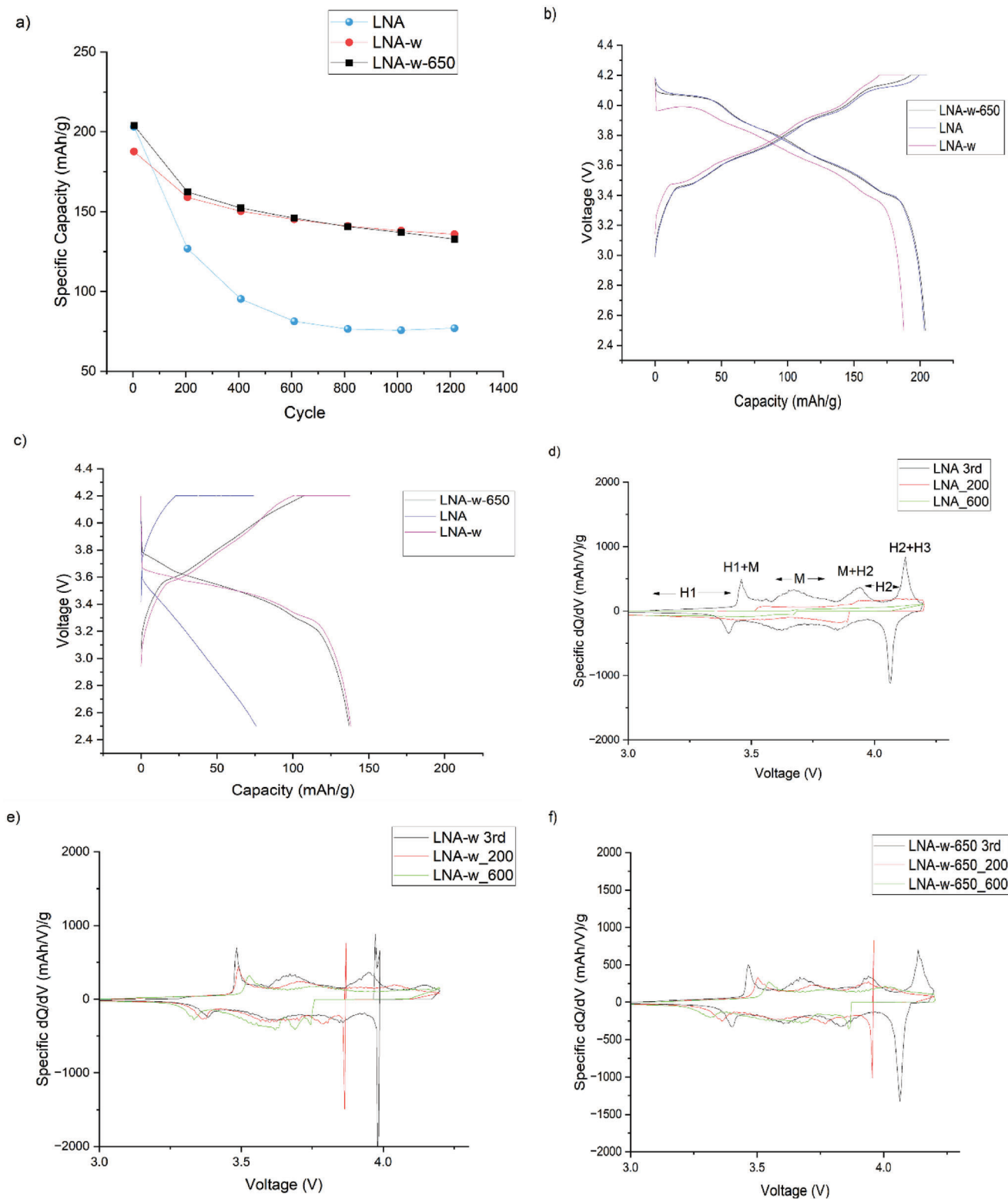
NANO · MICRO
small

www.small-journal.com

Figure 4. a) Specific discharge capacities at 0.2 C for every 100 cycles until 1200 cycles, b) first cycle voltage curve, c) last cycle voltage curve, d–f) differential capacity (dQ/dV) profiles for every 200 cycles for pristine (LNA), washed (LNA-w), and secondary heat-treated (LNA-w-650) samples, respectively.

**ADVANCED
SCIENCE NEWS**

www.advancedsciencenews.com

NANO · MICRO
small

www.small-journal.com

for LNA). However, the secondary heat treatment restored the capacity of LNA-w, increasing it to 203.9 mAh g^{-1}. As shown in Figure 4b, LNA-w had a higher initial charge voltage and a lower initial discharge voltage than LNA, confirming the lower conductivities of the material because of the NiO phase on the surface. However, Figure 4b also shows that LNA-w-650 and LNA had almost similar initial charge-discharge voltage profiles. This can be explained by the decrease in Ni^{2+} on the surface due to the secondary heat treatment (Figure 3f). During the first 200 cycles of the LNA cell, the capacity decreased from 203.1 mAh g^{-1} rapidly to 126.9 mAh g^{-1}. After 200 cycles, LNA-w and LNA-w-650 had better capacity retention (159.4 and 162.4, respectively). After 1200 cycles, the capacity retention results for LNA, LNA-w, and LNAw-650 were 77.5, 135.8, and 131.6 mAh g^{-1}, respectively. Full cells were tap charged at 4.2 V until the current decreased to 0.03 C. This type of charge is very harmful for LiNiO$_2$ cathode material because it increases high-volume lattice changes during a high-voltage H2 to H3 phase transitions.[24] The LiNiO$_2$ cathode material underwent multiple phase transitions during charge and discharge from the first hexagonal (H1) phase to the monoclinic (M) phase, the M phase to the H2 phase, and the H2 phase to the H3 phase.[25,26] These phase transitions are shown as peaks in Figure 4d. Washing seemed to improve the cyclability properties of the LNA-w cell. This could be explained by the lower ionic conductivity of the surface due to the presence of delithiated phase NiO, which suppressed the H2 to H3 phase transition.

Changes in H2 to H3 phase transition were confirmed by the differential capacity (dQ/dV) profiles shown in Figure 4d–f. For LNA and LNA-w-650, there were clear peaks for H2 to H3; for LNA-w, the peak almost totally disappeared. Additional dQ/dV profiles showed that, for LNA, the H2 to H3 peak completely disappeared after 200 cycles, and most of the phase transition peaks disappeared after 600 cycles. For LNA-w and LNA-w-650, H2 to H3 disappeared after 200 cycles; the other phase transition peaks remained. LNA's poor cyclability properties could be related to a high level of charging at high voltage and an increased amount of high-volume lattice changes during the H2 to H3 phase transition and a residual lithium reaction with electrolyte and gas formation during charging.
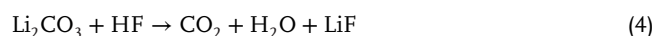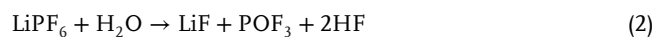
2.2. Gas Investigations during the Cell Cycling (GC-MS)

Figure 5 shows the gas measuring point in the voltage curve and the percentages of different gases produced during the first cycle charge and discharge, as measured by Gas chromatography-mass spectrometry (GC-MS). During the charge, the major gas components were carbon oxides, hydrocarbons, and carbonates. Jung et al.[27] proposed that, for high-nickel cathodes, CO$_2$/CO evolution primarily occurs because O$_2$ is released during the H2 to H3 phase transition and reacts with ethylene carbonate (EC) in the electrolyte according to Equation (1):[27,28]

$$EC + 2O_2 \rightarrow 2CO_2 + CO + 2H_2O \tag{1}$$
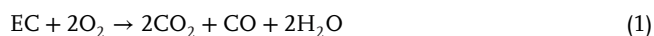
Moreover, residual lithium on the particle surface can oxidize and increase CO$_2$ production, which can explain the higher CO$_2$ production for LNA than for LNA-w and LNA-w-650 as shown in **Figure 6**a.[29,30]

As shown in Figures 5 and 6a, the main difference between the charge and discharge results was that, during discharge, fewer hydrocarbons were produced, and the total amount of gas was lower. The main difference between the studied samples was that cycling of LNA produced much more carbonyls, ethers, halogenated alkanes, and fluorosilanes than cycling of LNA-w and LNAw-650. Fluorosilanes indicated the amount of HF species formed when electrolyte salt lithium hexafluorophosphate (LiPF$_6$) reacts with water (H$_2$O) (Equation (2)) and can further attack transition metal (TM) oxide to produce slightly soluble TMF$_2$ and H$_2$O (Equation (3)).[31] Chemical decomposition of Li$_2$CO$_3$ with HF according to Equation (4) accelerate electrolyte decomposition reaction and increase CO$_2$ production.[27–31]

$$LiPF_6 + H_2O \rightarrow LiF + POF_3 + 2HF \tag{2}$$

$$TMO + 2HF \rightarrow TMF_2 + H_2O \tag{3}$$

$$Li_2CO_3 + HF \rightarrow CO_2 + H_2O + LiF \tag{4}$$

Fluorosilanes are detected because HF etches the protective methylsilyl layer on the GC column and forms fluorotrimethylsilane. Figure 6b shows the correlation between the fluorosilane species produced and the amount of residual lithium on the secondary particle surface, as measured by titration. The results clearly indicate that the residual lithium on the particle surface accelerated HF production.

2.3. Electrochemical Performances and Effects of the Charging Protocol

To clarify the effects of high voltage charging on electrochemical performance, new cells were tested without tap charge (CC) and a formation charge voltage limited to 4.1 V. The results were compared with the cell tested with tap charge (CCCV) (**Figure 7**a–f). For the cells tested without tap charge—LNA*, LNA-w*, and LNA-w-650*—the initial discharges were 193.8, 170.3, and 192.3 mAh g^{-1}, respectively. These results were ≈10 to 17 mAh g^{-1} lower than the results of the cells tested with tap charge. The cycling properties significantly improved for LNA*, with a capacity of 155.5 mAh g^{-1} (80.2% retention) after 1200 cycles compared to 77 mAh g^{-1} (38% retention) for LNA. The voltage profiles of LNA and LNA* (Figure 7b) were quite similar for the first cycle. After 1200 cycles, most of the LNA charge occurred in the tap charge mode and the discharge voltage dropped very fast; however, the voltage profiles for LNA* revealed normal voltage plateaus after 1200 cycles.

Despite LNA-w's higher initial capacity, the cycling stability levels of LNA-w* and LNA-w were quite similar. After 200 cycles, the capacities were at the same level; after 1200 cycles, LNA-w* and LNA-w had capacities of 139.4 and 135.9 mAh g^{-1}, respectively (Figure 7c). However, the discharge voltage after 1200 cycles was higher for LNA-w* than for LNA-w (Figure 7d). After 1200 cycles, LNA-w-650* had a better capacity (144.3 mAh g^{-1} (75.0% retention)) than LNA-w-650 (132.8 mAh g^{-1} (65.1% retention)). As shown in **Figure 8**a, the dQ/dV profile revealed that the H2 to H3 phase transition was more stable for LNA* than for LNA (Figure 4d). However, the H2 to H3 peak faded more than the
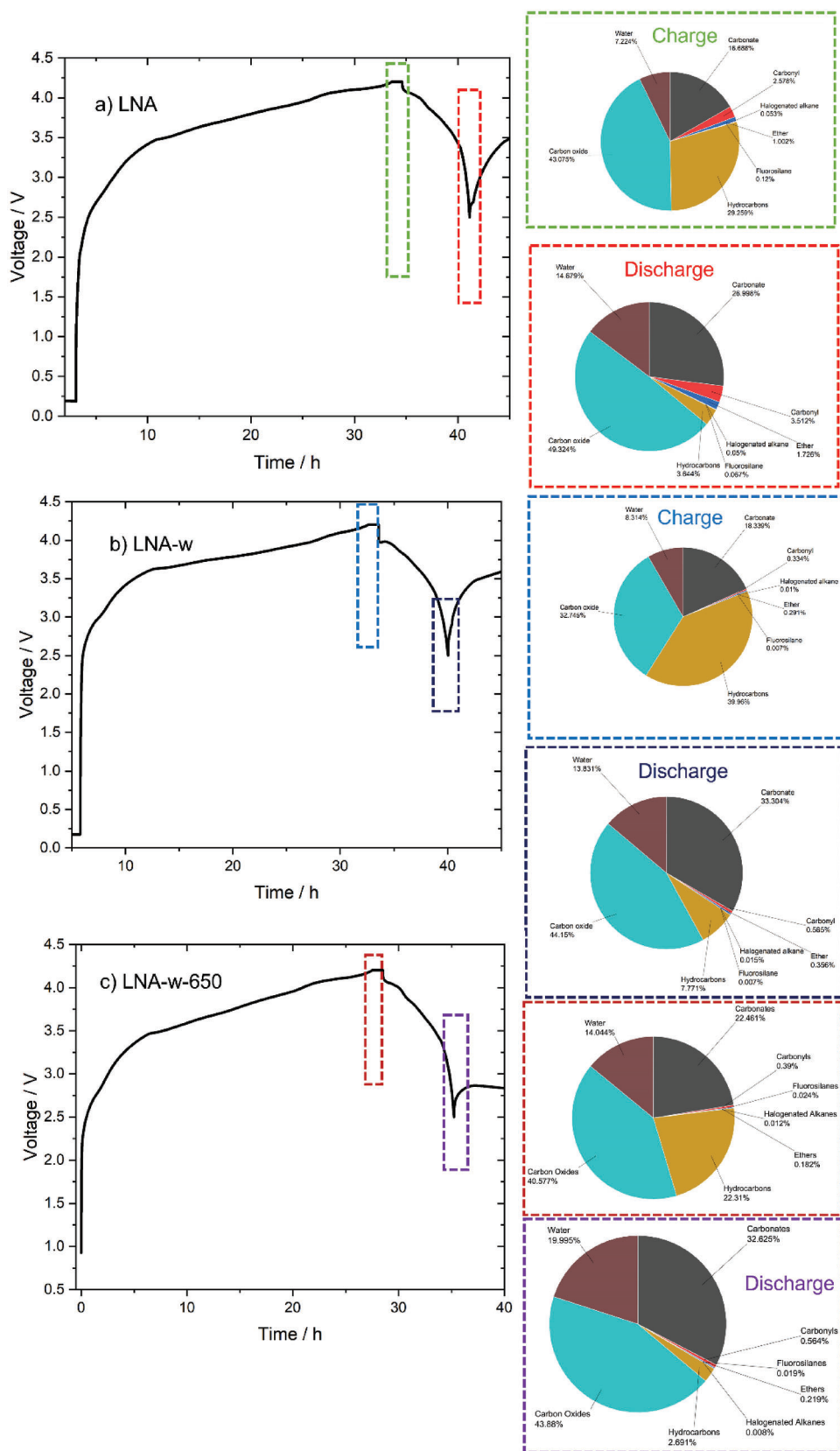
**ADVANCED
SCIENCE NEWS**

www.advancedsciencenews.com

NANO · MICRO

small

www.small-journal.com

Figure 5. The gas formulation during the charge–discharge voltage curve with marked measurement point and percentages of gases (detected by GCMS) of a) LNA, b) LNA-w, and c) LNA-w-650.
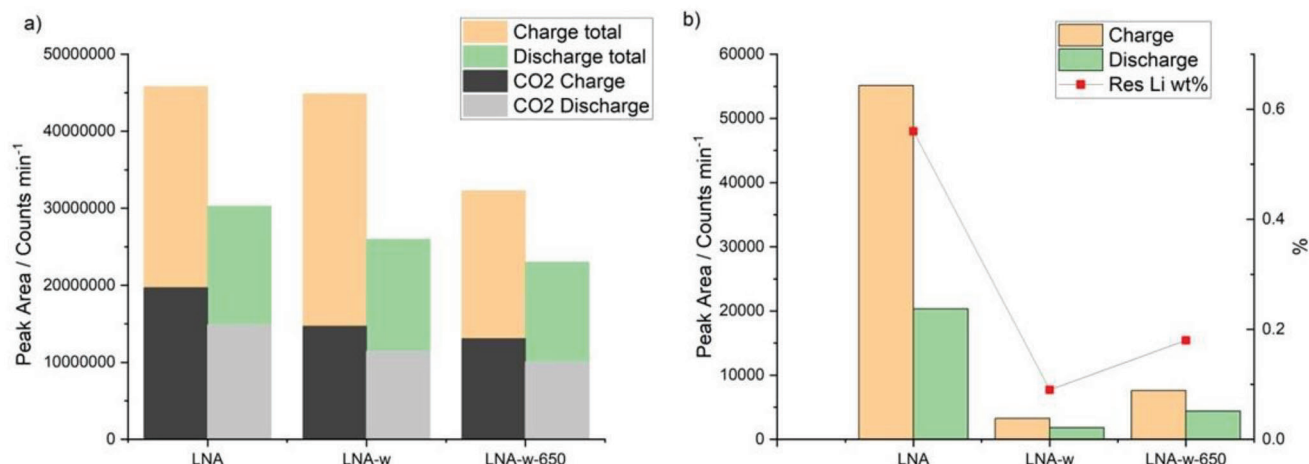
Figure 6. a) Sum areas of total/CO_2 gas produced during charge and discharge and b) amount of fluorosilane produced during charge and discharge (1st Y axis) and amount residual lithium wt%, as measured by titration (2nd Y axis).

other phase transition peaks during cycling, indicating that the H2 to H3 phase transition was the reason for the remaining capacity fading. As shown in Figure 8b, the dQ/dV profile for LNA-w* revealed that the H2 to H3 phase transition was suppressed by low surface conductivity. However, the phase transition peak for LNA-w-650* is clearly visible in Figure 8c, and it is more stable during cycling than for LNA-w-650 (Figure 4f).

3. Conclusion

In summary, we reported that how the process of washing residual lithium and performing a secondary heat treatment changes the material surface, chemical environment, and electrochemical performance of LNA cathode material for LIBs. During the washing process, impurities, and residual Li_2CO_3 and LiOH compounds were effectively removed from the LNA surface; however, this process also created a nonconductive delithiated NiO phase on the surface. Full cell tests revealed that this NiO phase decreased initial capacities from 204.1 to 187.6 mAh g^{-1} and suppressed high-volume lattice changes in the H2 to H3 phase transition at high voltages. Suppressing H2 to H3 phase transition for LNA-w showed enhanced cycle properties of 135.9 mAh g^{-1} after 1200 cycles, while unwashed LNA showed only 77 mAh g^{-1}. According to XPS studies, a secondary heat treatment at 650 °C after washing increased the amount of Ni^{3+} on the surface, indicating that the NiO phase was lithiated back to conductive LiNiO$_2$ and the initial capacity was restored to 203.9 mAh g^{-1} with an enhanced cycle life of 131.6 mAh g^{-1} after 1200 cycles.

LNA, LNA-w, and LNA-w-650 were tested without tap charge (CCCV mode) to avoid H2 to H3 phase transition at high voltages. The initial capacities decreased for all samples, as expected, and the cycle properties were enhanced, especially for LNA (which increased from 77 to 155.5 mAh g^{-1}). The capacities for LNA-w and LNA-w* after 1200 cycles were quite similar at 135.9 and 139.4 mAh g^{-1}, respectively, because the H2 to H3 phase transition had already been suppressed by the NiO phase. For LNA-w-650, the cycle properties were enhanced from 131.6 to 144.32 mAh g^{-1}. The findings revealed that the bad cycling properties of LiNiO$_2$ were related to a high-voltage second hexagonal

(H2) to third hexagonal (H3) phase transition. GC-MS analysis during charge and discharge revealed that LNA produced HF-related gases from the reaction of residual lithium and the electrolyte salt LiPF$_6$. This type of gas formation started at a high voltage and could explain the poor cycling properties of LNA compared to LNA-w-650, although both cells were charged at H2 to H3 phase transition voltages with the tap charge. Our studies provide investigations about secondary heat treatment of cobalt-free cathode chemistries LNA, which will be expected for next-generation cathodes for LIBs.

4. Experimental Section

Synthesis of Aluminum Modified LiNiO$_2$: Figure 1a shows the schematic illustration of cobalt-free LiNi$_{0.975}$Al$_{0.025}$O$_2$ (LNA) preparation process. The Ni(OH)$_2$ precursor was precipitated at 50 °C [32] and mixed with LiOH and Al(OH)$_3$ using a Li:Ni:Al molar ratio of 1.04:0.975:0.025 followed by calcination at 690 °C. Excess LiOH was used to compensate for the lithium loss during high-temperature calcination and to ensure homogeneous lithiation. The mixture was calcined with a 2.5 °C min^{-1} heating ramp and a 5 h holding time at 690 °C in an oxygen atmosphere and subsequently milled and sieved to less than 40 μm in dry room conditions. Three samples were prepared: LiNi$_{0.975}$Al$_{0.025}$O$_2$ (LNA), which was an unwashed sample; LNA-w, which was washed with a certain amount of de-ionized water and then filtered and dried at 180 °C under vacuum conditions; and LNA-w-650, which was washed, filtered and dried in the same manner as LNA-w and then underwent secondary heat treatment at 650 °C for three hours in an oxygen atmosphere.

Structural and Morphology Analysis: X-ray diffraction (XRD) was measured with Rigaku SmartLab 9 kW X-ray diffractometers (Rigaku Corporation, Tokyo, Japan) using Co as a source at 40 kV and 135 mA. Diffractograms were collected in the 2θ range (5–120° at 0.01° intervals) with a scan speed of 4.06° min^{-1}. Peaks were identified using the database from the International Centre for Diffraction Data (PDF-4 + 2022). A detailed description of the XRD analysis is provided in the earlier paper.[32] Rietveld refinement was carried out with the PDXL ver. 2 suite (Rigaku Corporation) using b-spline background correction and split pseudo-Voigt peak shape modeling against the target phase. The constraints used for modeling were as follows: the same temperature factors for Li 1s and Ni1 occupying the 3b site and the same temperature factors for site 3a occupied by Ni2 and Al ions. No vacancies for sites 3a and 3b were allowed (i.e., the total occupancy for each site was 1). The occupancy of oxygen ion was fixed,
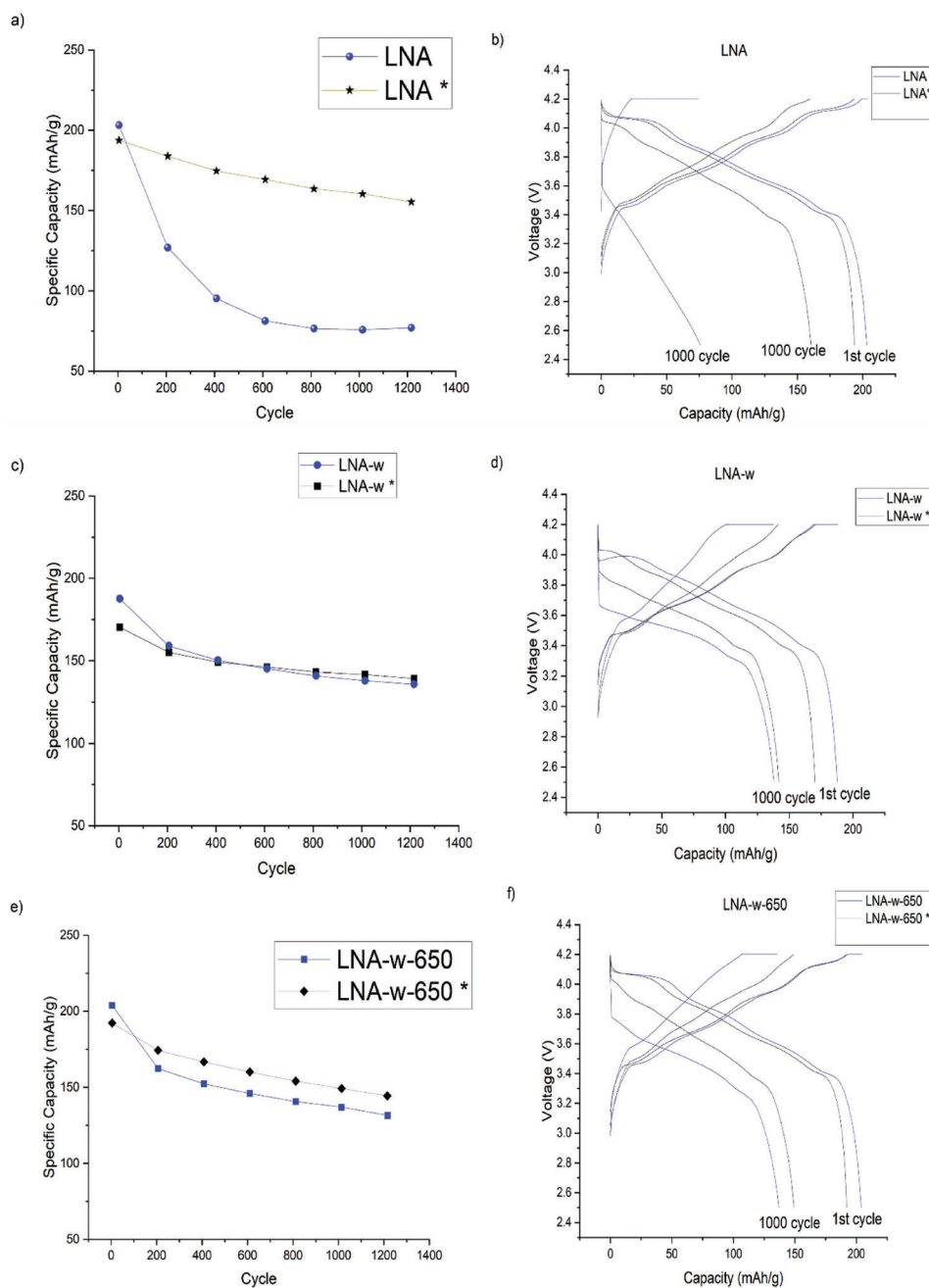
Figure 7. The specific discharge capacities of 0.2 C capacity check cycles and charge and discharge voltage profiles for the first cycle and after 1000 cycles for a,b) LNA and LNA*, c,d) LNA-w and LNA-w*, and e,f) LNA-w-650 and LNA-w-650*.

and its position was set as a free parameter. Occupancy of aluminum was obtained and fixed for the 3a site from ICP measurements of prepared materials, while Ni and Li ions were set as free parameters. Refinement continued until the parameters converged and changes in consecutive cycles were below a strict cutoff. In addition, the estimated standard deviation (ESD) was low for the obtained parameters, and the final Rwp was affected by Kb ghost peaks, which did not overlap with observed reflections.

The chemical environment at the surface area (thickness of <10 nm) was analyzed with X-ray photoelectron spectroscopy (XPS) using a Thermo Fisher Scientific ESCALAB 250Xi XPS system (Thermo Fisher Scientific, Waltham, MA, USA). The powder samples were placed on a gold sample holder, and the high-resolution scan used a pass energy of 20 eV, while the survey scan used a pass energy of 150 eV. The monochromatic Al Kα radiation (1486.7 eV) operated at 20 mA and 15 kV with an X-ray spot size of 900 µm. The Li, Ni, Al, O, and C were measured for all the samples, and the measurement data were analyzed with Avantage v.5 software (Thermo Fisher Scientific). The charge compensation was carried out by applying the C1s at 284.8 eV as a reference to determine the presented spectra and calibrate the binding energies.

The microstructures shown in the field-emission scanning electron microscopy (FESEM) images were obtained using a Zeiss Sigma FESEM (Zeiss Group, Oberkochen, Germany) operating at 5 kV.
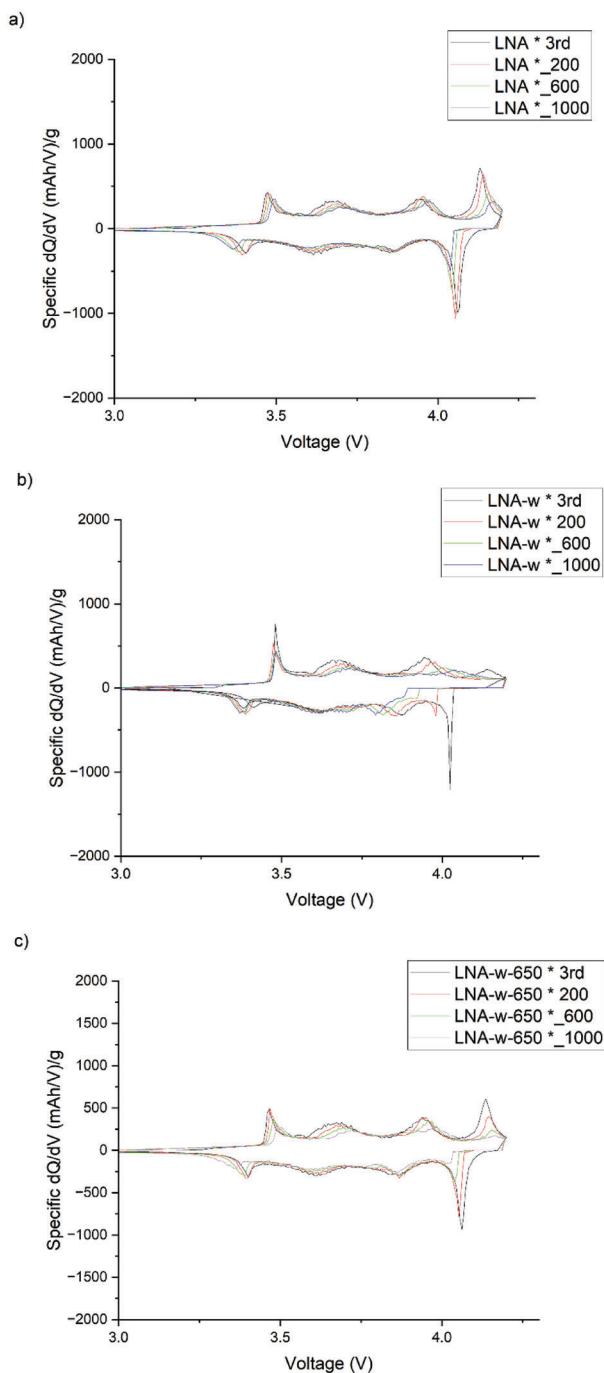
**ADVANCED
SCIENCE NEWS**

www.advancedsciencenews.com

**NANO · MICRO
small**

www.small-journal.com

Figure 8. Differential capacity (dQ/dV) profiles for every 200 cycles for a) LNA*, b) LNA-w*, and c) LNA-w-650*.

The ICP-OES determinations were carried out with an Agilent 5110 VDV ICP-OES (Agilent Technologies, Santa Clara, CA, USA) equipped with an SPS-4 autosampler, a U-series concentric glass nebulizer, a cyclonic glass double-pass spray chamber, and a 1.8 mm semi-demountable torch. The analysis results are given as the mean value of five replicated measurements. Yttrium (wavelength 371.029) was used as an internal standard to correct for sensitivity drift and matrix effects in the measurements.

Full Cell Assembly and Electrochemical Testing: Electrochemical performance testing was carried out using full cells with graphite as the anode material. All electrode foils and battery cells were prepared in dry room conditions. A cathode slurry was prepared with a ThinkyMixer ARE-250 (Thinky Corporation, Tokyo, Japan). The slurry composition was 4 wt% polyvinylidene fluoride (Kureha #1100), 4 wt% carbon (Timcal C45), and 92 wt% active material, with 1-methyl-2-pyrrolidinone (NMP, Alfa Aesar, anhydrous 99.5%) as a solvent. The slurry was spread on aluminum foil with 100 µm applicators before it was dried on a hot plate at 50 °C for 1 h and then placed in a vacuum oven at 120 °C overnight. The cathode foil was calendered three times before cell assembly. The active material loaded on the foil was about 12 mg cm^{-2} (1C = 250 mAh g^{-1}). For the full cells, the electrode pair pouch cell (50 mAh) was prepared with a graphite anode (Hitachi), an electrolyte of 1.15 M LiPF$_6$ in EC:DMC:EMC (ethylene carbonate, dimethyl carbonate, ethyl methyl carbonate) (2:4:4), and 1 wt% vinylene carbonate. Two programs were used for cell testing. The first program was performed with tap charge (e.g., constant current constant voltage (CCCV) mode). The formation cycle was charged to 4.2 V at 0.03 C and discharged to 2.5 V at 0.1 C. For the cycling tests, the cells were initially charged at a constant current of 0.5 C until 4.2 V was reached and then charged at a constant voltage until the current decreased to 0.03 C. After a 10 min rest, they were discharged to 2.5 V at 0.5 C. Every 200 cycles, a capacity check cycle at 0.2 C was run. Before each capacity checks, the cells were discharged at 0.2 C. The second program's formation cycle was only charged to 4.1 V at 0.03 C. In addition, 0.5 C cycling was performed without tap charge at 0.03 C (e.g., constant current (CC) mode).

Gas Chromatography-Mass Spectrometry (GC-MS) Analysis for Full Cells: Gas chromatography-mass spectrometry (GC-MS) analysis was conducted using a GCMS QP2010 Plus (Shimadzu) equipped with a TOPAZ SPME liner, a column guard (Restek, deactivated), a PLOT Q-bond (Restek) was used as an analytical column and a particle trap (Restek, deactivated) to protect the MS. Helium was used as carrier gas and a GC valve with a 500 µL sample loop ensured the transfer of the probe into the GC-MS. The GC valve and injector were kept at 80 °C. The electrodes were placed with a Celgard separator, an electrolyte of 1 M LiPF$_6$ in EC:EMC (3:7), and 2 wt% vinylene carbonate in a special cell for gas analysis manufactured by EL-CELL. For sampling, valves were opened, and a constant flow of helium carried the gas mixture to the sample loop. Shortly after the sampling, the valves were closed, and the cell remained without gas flow to avoid the electrolyte from drying. The cell was cycled between 2.5 and 4.2 V, and a 1 h CV step was used after the charge. The applied current corresponded to C-rates of 0.03 C for charge and 0.1 C for discharge. For the analysis of the gas mixture, a sample was extracted at 4.2 V after charging and at 2.5 V after discharging.

Supporting Information

Supporting Information is available from the Wiley Online Library or from the author.

Acknowledgements

Conflict of Interest

The authors declare no conflict of interest.

Data Availability Statement

The data that support the findings of this study are available from the corresponding author upon reasonable request.

Keywords

[1] K. Mizushima, P. C. Jones, P. J. Wiseman, J. B. Goodenough, *Mater. Res. Bull.* **1980**, *15*, 783.

[2] H. Cavers, P. Molaiyan, M. Abdollahifar, U. Lassi, A. Kwade, *Adv. Energy Mater.* **2022**, *12*, 2200147.

[3] Z. Guo, Z. Cui, R. Sim, A. Manthiram, *Small* **2023**, 2305055.

[4] A. Pokle, D. Weber, M. Bianchini, J. Janek, K. Volz, *Small* **2023**, *19*, 2205508.

[5] H. Li, L. Wang, Y. Song, Y. Wu, H. Zhang, A. Du, X. He, *Small* **2023**, *19*, 2302208.

[6] M. M. E. Cormier, N. Zhang, A. Liu, H. Li, J. Inglis, J. R. Dahn, *J. Electrochem. Soc.* **2019**, *166*, A2826.

[7] H. J. Noh, S. Youn, C. S. Yoon, Y. K. Sun, *J. Power Sources* **2013**, *233*, 121.

[8] T. Ohzuku, A. Ueda, M. Nagayama, *J. Electrochem. Soc.* **1993**, *140*, 1862.

[9] C. Delmas, M. Ménétrier, L. Croguennec, I. Saadoune, A. Rougier, C. Pouillerie, G. Prado, M. Grüne, L. Fournès, *Electrochim. Acta* **1999**, *45*, 243.

[10] R. Pan, E. Jo, Z. Cui, A. Manthiram, *Adv. Funct. Mater.* **2023**, *33*, 2211461.

[11] H. Arai, *Solid State Ionics* **1995**, *80*, 261.

[12] H. Liu, Y. Yang, J. Zhang, *J. Power Sources* **2006**, *162*, 644.

[13] J. Kim, Y. Hong, K. S. Ryu, M. G. Kim, J. Cho, *Electrochem. Solid-State Lett.* **2006**, *9*, A19.

[14] G. V. Zhuang, G. Chen, J. Shim, X. Song, P. N. Ross, T. J. Richardson, *J. Power Sources* **2004**, *134*, 293.

[15] M. Metzger, B. Strehle, S. Solchenbach, H. A. Gasteiger, *J. Electrochem. Soc.* **2016**, *163*, A1219.

[16] P. Molaiyan, S. E. Mailhiot, K. Voges, A. M. Kantola, T. Hu, P. Michalowski, A. Kwade, V. V. Telkki, U. Lassi, *Mater. Des.* **2023**, *227*, 111690.

[17] D. H. Cho, C. H. Jo, W. Cho, Y. J. Kim, H. Yashiro, Y. K. Sun, S. T. Myung, *J. Electrochem. Soc.* **2014**, *161*, A920.

[18] W. Zhang, C. Yuan, J. Zhu, T. Jin, C. Shen, K. Xie, *Adv. Energy Mater.* **2023**, *13*, 2202993.

[19] J. Välikangas, P. Laine, M. Hietaniemi, T. Hu, M. Selent, P. Tynjälä, U. Lassi, *J. Solid State Electrochem.* **2023**, *27*, 641.

[20] S. Ahmed, P. A. Nelson, K. G. Gallagher, N. Susarla, D. W. Dees, *J. Power Sources* **2017**, *342*, 733.

[21] C. S. Yoon, D. W. Jun, S. T. Myung, Y. K. Sun, *ACS Energy Lett.* **2017**, *2*, 1150.

[22] X. Xiong, Z. Wang, P. Yue, H. Guo, F. Wu, J. Wang, X. Li, *J. Power Sources* **2013**, *222*, 318.

[23] A. M. Andersson, D. P. Abraham, R. Haasch, S. MacLaren, J. Liu, K. Amine, *J. Electrochem. Soc.* **2002**, *149*, A1358.

[24] H. H. Ryu, K. J. Park, C. S. Yoon, Y. K. Sun, *Chem. Mater.* **2018**, *30*, 1155.

[25] H. Li, N. Zhang, J. Li, J. R. Dahn, *J. Electrochem. Soc.* **2018**, *165*, A2985.

[26] W. Li, J. N. Reimers, J. R. Dahn, *Solid State Ionics* **1993**, *67*, 123.

[27] R. Jung, M. Metzger, F. Maglia, C. Stinner, H. A. Gasteiger, *J. Electrochem. Soc.* **2017**, *164*, A1361.

[28] A. T. S. Freiberg, J. Sicklinger, S. Solchenbach, H. A. Gasteiger, *Electrochim. Acta* **2020**, *346*, 136271.

[29] J. K. Papp, N. Li, L. A. Kaufman, A. J. Naylor, R. Younesi, W. Tong, B. D. McCloskey, *Electrochim. Acta* **2021**, *368*, 137505.

[30] S. S. Zhang, *Front. Energy Res.* **2014**, *2*, 59.

[31] S. Jamil, G. Wang, M. Fasehullah, M. Xu, *J. Alloys Compd.* **2022**, *909*, 164727.

[32] J. Välikangas, P. Laine, M. Hietaniemi, T. Hu, P. Tynjälä, U. Lassi, *Appl. Sci.* **2020**, *10*, 8988.

2305349 (11 of 11)